Nanoscale Advances

ROYAL SOCIETY OF CHEMISTRY

COMMUNICATION

View Article Online
View Journal

Cite this: DOI: 10.1039/d5na01149c

Received 19th December 2025
Accepted 30th March 2026

DOI: 10.1039/d5na01149c

rsc.li/nanoscale-advances

Extended seed-mediated silver nanorods: co-solvent mediated synthesis and plasmon mode reassignment

Jun Zhu, † Ruixue Chen,† Alexander Al-Feghali, Amy Szuchmache Blum and R. Bruce Lennox*

Improvements to published reports of the seed-mediated synthesis of silver nanorods (AgNRs) are reported. These improvements include the application of a depletion purification process to facilitate the assignment of the transverse surface plasmon resonances (TSPR) of AgNRs and access to increased lengths of the AgNRs by increasing the solubility of the reaction intermediate, CTA–Ag–Br.

Gold and silver nanomaterials have been the subject of considerable investigation due to their rather unique optical properties that lead to potential applications in optical sensors,[1] photocatalysis,[1,2] plasmonic nanocircuits,[3] antibacterial products,[4] and quantum plasmonic systems.[5] A commonly used entry into the synthesis of morphologically asymmetric gold nanoparticles (AuNPs) such as rods, plates, and tetrahedra involves the use of growth from an initial solution population of spherically symmetric NPs or seeds. The seed-mediated growth method pioneered by Murphy and El-Sayed has been particularly effective in achieving precise control of both the size and aspect ratio (AR; length : width ratio) of gold nanorods (AuNRs)[6,7] and several methodologies have been reported for the preparation of both AgNRs and silver nanowires (AgNWs),[8] including the thermal reshaping of Ag decahedra,[9] the polyol method,[10] light-assisted synthesis,[11,12] and the seed-mediated growth method.[13] Seed-mediated methods using Au nanoparticle seeds[13] or palladium (Pd) nanoparticle seeds[14] have been established by Wang and Liz-Marzán for AgNR preparation.[15,16] However, the preparation of AgNRs with relatively short lengths and small diameters (<30 nm) remains challenging.[17,18] Moreover, the documented methods also involve considerable experimental complexity, perhaps hindering a full exploration of their application.

AgNRs synthesized *via* the seed-mediated method first introduced by Murphy are particularly appealing due to their relatively facile control of NR length and associated longitudinal surface plasmon resonance (LSPR) outcome, through the variation of the seed quantity.[13,19] AgNRs thus prepared have an aspect ratio of 3.5 to 10 and diameters of 12 to 20 nm, characteristics that are of particular interest in photothermal applications[20] and optoacoustic imaging.[21] However, AuNRs prepared using a similar seed-mediated methodology exhibit a weak transverse SPR (TSPR) around 510 nm and a strong LSPR signal in the 600–850 nm range.[22] AgNRs prepared using this synthesis methodology exhibit a strong absorbance at 420 nm (assigned to a TSPR) and a strong absorbance in the range of 470 to 665 nm (assigned to a LSPR).[13,19,23,24] Calculations however suggest that AgNRs whose diameters are <30 nm should have TSPR peaks <400 nm.[14] On the other hand, the absorbance observed at around 410 nm in the polyol synthesis of silver nanowires (AgNWs; width of 30 to 40 nm) has been assigned to AgNP impurities.[25,26] After removal of these AgNPs from the desired AgNWs, an absorbance shoulder at 350 nm and a strong peak at 380 nm emerge. These were respectively assigned to the SPR of bulk silver and the TSPR of NWs.[25,26] Similarly, Murphy *et al.* synthesized AgNWs with widths of 35 nm using a seedless method and reported a resulting TSPR peak at around 370 nm.[27] Although absorbance maxima at 350 nm and 380 nm have been reported in several studies,[28–30] to date a consensus assignment of these peaks has not emerged.

We report here the use of the depletion purification method in AgNR syntheses that had previously been used in the purification of AuNRs[31] and gold nanotriangles (AuNTs).[32] This is necessary because unlike the case of AgNWs, where the AgNP impurities can be readily removed by centrifugation because of the large differences in size/mass, AgNP impurities in AgNR syntheses cannot be removed by centrifugation and thus require alternate separation strategies. In parallel, increasing the solubility of the reaction's key silver intermediate (a CTA–Ag–Br complex), by addition of small quantities of a cosolvent, is shown to increase the AgNR length to 224 ± 77 nm from 97.3 ± 8.5 nm and extend the resulting LSPR signal to 850 nm from the previous limit of 665 nm.

Department of Chemistry and Quebec Center for Advanced Materials (QCAM), McGill University, 801 Sherbrooke St. West, Montreal, QC H3A 0B8, Canada. E-mail: bruce.lennox@mcgill.ca

† Both authors contributed equally to this work.

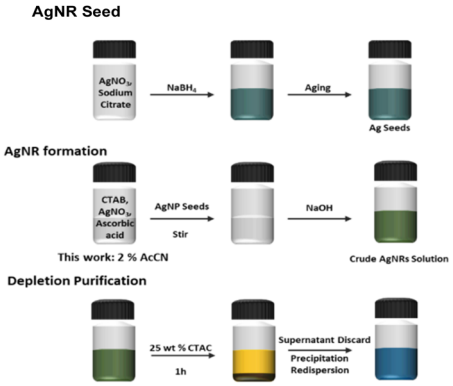

Scheme 1 Schematic of the typical steps in the seed-mediated AgNR synthesis. A co-solvent (2% acetonitrile) is added in the modified seed mediated AgNR synthesis reported here in order to enhance solubility of the key reaction intermediate – the CTA–Ag–Br complex.

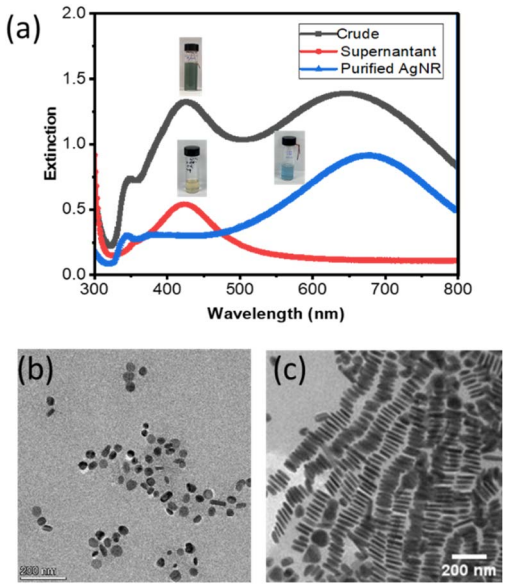

Fig. 1 UV-vis spectroscopy and TEM characterization of AgNRs. (a) UV-vis spectra of AgNRs before (crude) and after (supernatant and purified AgNRs) application of depletion purification. TEM images of (b) the supernatant AgNPs separated from AgNRs in the depletion purification process and (c) AgNRs obtained *via* the depletion purification process.

AgNRs were synthesized using the seed mediated methodology following a published procedure (Scheme 1).[13] AgNP seeds were prepared by reducing $AgNO_3$ with $NaBH_4$ in trisodium citrate solution (Fig. S1). The growth solution was prepared by mixing 0.025 mL of 50 mM $AgNO_3$ and 0.25 mL of 100 mM ascorbic acid into 5 mL of 80 mM cetyltrimethylammonium bromide (CTAB) solution. In a typical synthesis, 0.05 mL of the seed solution was added to the growth solution, followed by the addition of 0.05 mL of 1 M NaOH to initiate the formation of AgNRs. The dark green crude AgNR solution was centrifuged at 6000*g* for 5 min to remove excess CTAB and ascorbic acid. After discarding the supernatant, the crude AgNR sample was redispersed in 5 mL of a 1 mM CTAB solution. Note that a white precipitate is observed after mixing $AgNO_3$ into the CTAB solution during the preparation of the growth solution and a layer of white precipitate exists after the product formation. The formation of this white precipitate not only reduces the yield of AgNRs, but is also observed to limit the aspect ratio of the resulting AgNRs.

Micron-long AgNWs have been shown to be readily separated from the small AgNP impurities (diameter 30–50 nm) by centrifugation.[25,26] This centrifugation method cannot however be applied to efficiently separate AgNRs from AgNPs. Given the successful use of the depletion method to induce shape and size selection separation of AuNPs from AuNRs[31] or AuNTs,[32] we applied this separation method to the AgNR samples prepared here. AgNRs thus precipitated within 1 hour after the addition of 1 mL of a 25 wt% CTAC solution to the crude AgNR dispersion. After decanting the pale-yellow supernatant, the AgNRs were redissolved in 5 mL of water to give a clear, blueish solution for further characterization.

The progress of the AgNR purification process was monitored using UV-vis spectroscopy (Fig. 1a) and TEM. TEM images establish that the AgNRs formed have an aspect ratio of 5.5 ± 1.0 (diameter = 17.6 ± 1.9 nm; length = 97.3 ± 8.5 nm). Importantly, the widths of these AgNRs is smaller (<20 nm) than those of AgNRs reported using other methods.[9–11,14,16] These results demonstrate the effectiveness of the depletion purification process in the preparation of morphologically uniform AgNR samples where >95% of the Ag is in the form of AgNRs (Fig. 1c).

The crude AgNR sample features absorbances at 350 nm (shoulder), 420 nm (previously assigned to the TSPR of AgNRs;[19,33]), and 665 nm (assigned to the AgNR LSPR;[13,19,33]). After purification, the pale-yellow supernatant exhibits a single absorbance peak at 420 nm. TEM images establish that this supernatant solely contains AgNP impurities (Fig. 1b). The isolated AgNR sample retains the same LSPR band at 665 nm as that of the crude AgNR solution. However, a sharp peak at 350 nm and a broad peak at 370 nm are also present. Neither are apparent in the unpurified sample because the absorbance of ascorbic acid and AgNP impurities (Fig. 1a) masks them in the spectra of the crude, as-prepared sample. Removal of the residual ascorbate and AgNP impurities in the purification process thus establishes that the 350 nm and 370 nm peaks are nanomaterial-related.

A previous mechanistic study of the seed-mediated AuNR synthesis concluded that the final aspect ratio of the AuNRs is limited by solubility of the reaction CTA–Ag–Br intermediate.[22] Noting that the AgNR LSPR band is limited to about 665 nm when using the original seed-mediated method[13] and that a white precipitate arises in the growth solution after AgNR formation, we reasoned that the AgNR synthesis likely proceeds *via* the same CTA–Ag–Br intermediate and is thus subject to the same solubility limitations. Although binary surfactants, such as CTAB/cetyldimethylbenzylammonium chloride,[7] CTAB/sodium oleate,[34] or CTAB:1-decanol,[35] have been applied to improve the solubility of reaction intermediates, their use

introduces additional experimental complexity. Given this, a simple co-solvent approach was employed using the addition of acetonitrile (2% final concentration) to the reaction mixture. This yields significantly longer AgNRs (Fig. S3; 224 ± 77 nm), an LSPR that extends to 850 nm (Fig. S2), and the two characteristic peaks at 350 nm and 370 nm.

The attribution of the 350 nm and 370 nm absorbances to the TSPR of the AgNRs is supported by Finite Difference Time Domain (FDTD) simulations.[25,26] In these simulations, AgNRs are modelled as cylinders with two hemispherical ends. When the experimentally observed dimensions of the AgNRs are used as inputs in the simulations (97.3 nm length and 17.6 nm width), the resulting FDTD simulated UV-vis spectrum exhibits two distinct bands at 350 nm and 370 nm (Fig. 2a), in excellent agreement with the experimental spectrum (Fig. 1a). Additional FDTD simulations using a range of lengths (88.8 nm to 105.8 nm) and widths (15.7 nm to 19.5 nm) establish that these absorbance maxima are quite insensitive to the precise NR lengths and widths (SI, Fig. S4).

The local charge density oscillations in the transverse direction of AgNRs are shown in Fig. 2b–e. Fig. 2b and c and present the field propagating along the *z*-axis and polarized along the *x*-*y* axis of the AgNRs at 350 nm. The collective oscillation of the charges follows an out-of-plane quadrupolar resonance mode. The field enhancement at the plasmon resonance at 370 nm is presented in Fig. 2d and e. The resonance peak can be labelled as dipolar resonance based on the symmetries of the distribution.

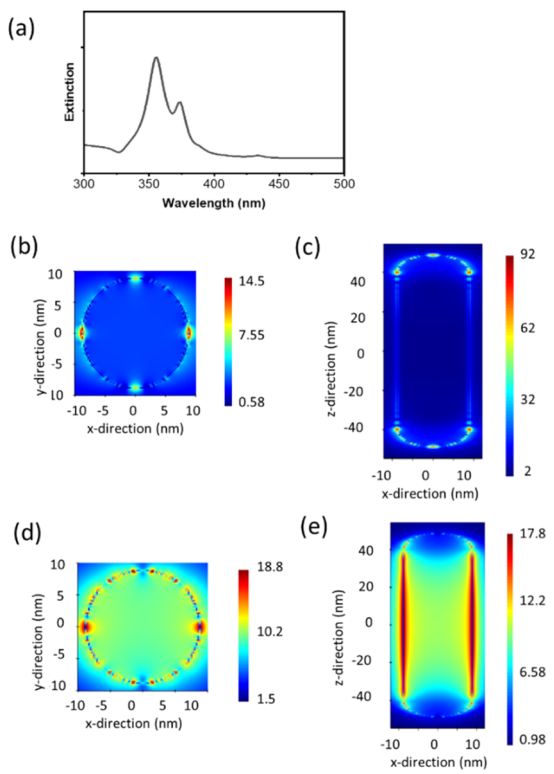

Fig. 2 FDTD simulations of the TSPR of an AgNR with a length of 97.3 nm and width of 17.6 nm. (a) Calculated UV-vis spectrum of AgNRs in the wavelength range of 300–500 nm. (b) and (c) The field profiles of the top view and side view indicating the out-of-plane quadruple mode (350 nm); (d) and (e) the field profiles of the top view and side view of the dipolar resonance (370 nm) mode.

Conclusions

In summary, we have refined the seed-mediated synthesis of AgNRs to enable access to samples with greater physical lengths and longer wavelength LSPR peaks. Adjustment of the solubility of the CTA–Ag–Br complex intermediate with limited quantities of the co-solvent acetonitrile yields AgNRs with LSPR maxima of 850 nm. Application of the depletion purification method verifies an assignment of the 420 nm absorbance to NP impurities, and FDTD simulations provide for an assignment of AgNR 350 nm and 370 nm absorbance maxima to TSPR.

Conflicts of interest

There are no conflicts to declare.

Data availability

The data supporting this article have been included as part of the supplementary information (SI). Supplementary information: experimental section, FDTD simulation, UV-Vis spectra, and TEM image. See DOI: https://doi.org/10.1039/d5na01149c.

Notes and references

1 Y. Hang, A. Wang and N. Wu, *Chem. Soc. Rev.*, 2024, **53**, 2932–2971.
2 S. Sarina, E. R. Waclawik and H. Zhu, *Green Chem.*, 2013, **15**, 1814–1833.
3 T. J. Davis, D. E. Gómez and A. Roberts, *Nanophotonics*, 2017, **6**, 543–559.
4 Z.-m. Xiu, Q.-b. Zhang, H. L. Puppala, V. L. Colvin and P. J. J. Alvarez, *Nano Lett.*, 2012, **12**, 4271–4275.
5 M. S. Tame, K. R. McEnery, Ş. K. Özdemir, J. Lee, S. A. Maier and M. S. Kim, *Nat. Phys.*, 2013, **9**, 329–340.
6 N. R. Jana, L. Gearheart and C. J. Murphy, *J. Phys. Chem. B*, 2001, **105**, 4065–4067.
7 B. Nikoobakht and M. A. El-Sayed, *Chem. Mater.*, 2003, **15**, 1957–1962.
8 B. Wiley, Y. Sun and Y. Xia, *Acc. Chem. Res.*, 2007, **40**, 1067–1076.
9 B. Pietrobon, M. McEachran and V. Kitaev, *ACS Nano*, 2009, **3**, 21–26.
10 J. Patarroyo, A. Genç, J. Arbiol, N. G. Bastús and V. Puntes, *Chem. Commun.*, 2016, **52**, 10960–10963.
11 J. Zhang, M. R. Langille and C. A. Mirkin, *Nano Lett.*, 2011, **11**, 2495–2498.
12 M. R. Langille, M. L. Personick and C. A. Mirkin, *Angew. Chem., Int. Ed.*, 2013, **52**, 13910–13940.
13 N. R. Jana, L. Gearheart and C. J. Murphy, *Chem. Commun.*, 2001, 617–618, DOI: 10.1039/B100521I.

14 M. Luo, H. Huang, S.-I. Choi, C. Zhang, R. R. d. Silva, H.-C. Peng, Z.-Y. Li, J. Liu, Z. He and Y. Xia, *ACS Nano*, 2015, **9**, 10523–10532.
15 X. Zhuo, X. Zhu, Q. Li, Z. Yang and J. Wang, *ACS Nano*, 2015, **9**, 7523–7535.
16 A. Sánchez-Iglesias, X. Zhuo, W. Albrecht, S. Bals and L. M. Liz-Marzán, *ACS Mater. Lett.*, 2020, **2**, 1246–1250.
17 R. R. da Silva, M. Yang, S.-I. Choi, M. Chi, M. Luo, C. Zhang, Z.-Y. Li, P. H. C. Camargo, S. J. L. Ribeiro and Y. Xia, *ACS Nano*, 2016, **10**, 7892–7900.
18 D. M. Eisele, H. v. Berlepsch, C. Böttcher, K. J. Stevenson, D. A. Vanden Bout, S. Kirstein and J. P. Rabe, *J. Am. Chem. Soc.*, 2010, **132**, 2104–2105.
19 C. J. Orendorff, L. Gearheart, N. R. Jana and C. J. Murphy, *Phys. Chem. Chem. Phys.*, 2006, **8**, 165–170.
20 L. M. Maestro, P. Haro-González, A. Sánchez-Iglesias, L. M. Liz-Marzán, J. García Solé and D. Jaque, *Langmuir*, 2014, **30**, 1650–1658.
21 Y.-S. Chen, Y. Zhao, S. J. Yoon, S. S. Gambhir and S. Emelianov, *Nat. Nanotechnol.*, 2019, **14**, 465–472.
22 J. Zhu and R. B. Lennox, *ACS Appl. Nano Mater.*, 2021, **4**, 3790–3798.
23 W. Zhang, X. Qiao, Q. Chen, Y. Cai and H. Chen, *Appl. Surf. Sci.*, 2012, **258**, 5909–5913.
24 M. R. Hormozi-Nezhad, M. Jalali-Heravi, H. Robatjazi and H. Ebrahimi-Najafabadi, *Colloids Surf., A*, 2012, **393**, 46–52.
25 Y. Sun, B. Gates, B. Mayers and Y. Xia, *Nano Lett.*, 2002, **2**, 165–168.
26 Y. Sun, Y. Yin, B. T. Mayers, T. Herricks and Y. Xia, *Chem. Mater.*, 2002, **14**, 4736–4745.
27 K. K. Caswell, C. M. Bender and C. J. Murphy, *Nano Lett.*, 2003, **3**, 667–669.
28 B. Liu, H. Yan, S. Chen, Y. Guan, G. Wu, R. Jin and L. Li, *Nanoscale Res. Lett.*, 2017, **12**, 212.
29 P. Meenakshi, R. Karthick, M. Selvaraj and S. Ramu, *Sol. Energy Mater. Sol. Cells*, 2014, **128**, 264–269.
30 M. Parente, M. van Helvert, R. F. Hamans, R. Verbroekken, R. Sinha, A. Bieberle-Hütter and A. Baldi, *Nano Lett.*, 2020, **20**, 5759–5764.
31 K. Park, H. Koerner and R. A. Vaia, *Nano Lett.*, 2010, **10**, 1433–1439.
32 J. Zhu and R. B. Lennox, *ACS Appl. Nano Mater.*, 2024, **7**, 23288–23294.
33 C. R. Rekha, V. U. Nayar and K. G. Gopchandran, *J. Sci. Adv. Mater. Devices*, 2018, **3**, 196–205.
34 X. Ye, C. Zheng, J. Chen, Y. Gao and C. B. Murray, *Nano Lett.*, 2013, **13**, 765–771.
35 G. González-Rubio, V. Kumar, P. Llombart, P. Díaz-Núñez, E. Bladt, T. Altantzis, S. Bals, O. Peña-Rodríguez, E. G. Noya, L. G. MacDowell, A. Guerrero-Martínez and L. M. Liz-Marzán, *ACS Nano*, 2019, **13**, 4424–4435.

